International Journal of Plasticity 85 (2016) 172–189

Contents lists available at ScienceDirect

International Journal of Plasticity

journal homepage: www.elsevier.com/locate/ijplas

New insight into the stable grain size of nanotwinned Ni in steady-state creep: Effect of the ratio of effective-to-internal stress

J. Li, J.Y. Zhang*, G. Liu**, J. Sun

State Key Laboratory for Mechanical Behavior of Materials, Xi'an Jiaotong University, Xi'an, 710049, PR China

ARTICLE INFO

Article history:
Received 18 March 2016
Received in revised form 28 June 2016
Available online 27 July 2016

Keywords:
A. Creep
A. Grain boundaries
A. Twinning
B. Structures
B.Metallic material

ABSTRACT

Understanding the underlying physical mechanisms of grain growth/refinement in materials, in particular for nanotwinned (NT) metals with high stacking fault energy (SFE), to manipulate their microstructural stability for performance optimization is a grand challenge in the material community. The characteristic stable grain sizes of metals have been modeled in terms of various physical parameters, whereas there remains a lack of quantitative information regarding the correlation of stable grain size with the underlying mechanism(s) in the light of competition between effective and internal stresses. In this work, we systematically investigated the microstructural evolution of high SFE NT Ni at different loading rates during room temperature creep. It is found that both grain growth at low stresses and grain refinement at high stresses achieved via (de)twinning-mediated processes emerge in NT Ni. Unlike the general belief that the steady-state grain sizes are characteristics of single-phase metals, it is appealing that the stable grain size is strongly dependent on the effective stress. The effective-to-internal stress ratio η_{Stress} plays a critical role in the grain size evolution: grains grow at $\eta_{Stress} < 1$, while they refine at $\eta_{Stress} > 1$. A stable grain size is reached at $\eta_{Stress} = 1$. We further developed a dislocation-based unified model to quantitatively predict the stable grain size of NT Ni achieved in steady-state creep and the steady-state creep strain rate from the perspective of effective stress, which gains insight into plastic deformation processes associated with growth or refinement of grains.

1. Introduction

Nanotwinned (NT) materials with twin thickness (λ) < 100 nm, are particularly attractive for structural applications because they possess high strength and simultaneously considerable ductility (Anderoglu et al., 2010; Lu et al., 2009a; Zhu et al., 2015; Wang et al., 2012), two characteristics that are traditionally considered to be mutually exclusive and are closely correlated with their internal microstructures, such as grain boundaries (GBs), twin boundaries (TBs) and dislocations. To date, some investigators reported the superior stability of medium stacking fault energy (SFE, γ ~45 mJ m^{-2}) NT Cu with grain size (d) in the submicron regime (Lu et al., 2009a), whereas others uncovered the (de)twinning-mediated grain growth via GB and/or TB motion/migration in nanocrystalline (NC) NT Cu (Brons et al., 2013; Wang et al., 2013), even in fatigued NT

* Corresponding author. Fax: +86 (0)2982663453.
** Corresponding author. Fax: +86 (0)2982663453.
E-mail addresses: jinyuzhang1002@mail.xjtu.edu.cn (J.Y. Zhang), lgsammer@mail.xjtu.edu.cn (G. Liu).

http://dx.doi.org/10.1016/j.ijplas.2016.07.009
0749-6419/

Ni–Fe (Cheng et al., 2010) and tensile deformed NT Ni with high SFE (γ ~125 mJ m^{-2}) (Li et al., 2015). Compared with NT metals, similar phenomena have been unambiguously confirmed in their nontwinned siblings (Gianola et al., 2006; Rupert et al., 2009; Li et al., 2009); namely coarse-grained (CG) and ultrafine-grained (UFG) materials are more favorable to suffer from grain refinement dominated by dislocation activities and deformation twinning, while NC materials are more prone to suffer from grain growth via the formation of nanotwins, in particular under severe plastic deformation. However, no detailed micromechanisms at the physical level are available to illustrate how these GBs migrate through twinning as well as its reverse process, *i.e.*, detwinning, to achieve the coalescence of nanograins in these nanostructured (including NT and NC) face-centered cubic (FCC) metals.

Most importantly, these results mentioned above suggest that both NC and NT metals have a stable grain size (d_s) at steady state, which is generally believed to be a characteristic of each metal and very important to engineering materials. To date, the stable grain sizes in NC metals achieved during plastic deformation can be predicted by some theoretical models using material parameters (Mohamed, 2003; Edalati and Horita, 2011), such as hardness, atomic bond energy, melting temperature, diffusivity and SFE. Specifically, Mohamed (2003) proposed a dislocation-based model to quantitatively capture the correlation between d_s and physical parameters for pure metals processed by ball milling, given the similarities of ball milling and creep. Therefore, it is normally anticipated that d_s can be obtained once the steady-state creep strain rate ($\dot{\varepsilon}_{SC}$) is reached during creep. More details are shown by Mohamed (2003) and will not be presented here. Moreover, Mohamed's model seems to be applicable to predict d_s in other deformation processes, such as HPT and ECAP, because the occurrence of a steady state is also attributed to the balance between dislocation accumulation and grain refinement on the one hand, and dislocation annihilation and grain growth on the other (Edalati and Horita, 2011). However, it is a pity that this well-accepted model as well as others (Edalati and Horita, 2011; Eckert et al., 1992) ignores an important fact that due to the microstructural evolution in deformed pure metals, both ball milling (or HPT and ECAP) and creep process would unavoidably give rise to notable (long-range and short-range) internal stresses, which reflect variations in the structural parameters that control the deformation process (Ahlquist et al., 1970). The usage of applied stress (σ_a) in Mohamed's model renders that the roles of average internal stress (σ_i) driving recovery or average effective stress ($\sigma_e = \sigma_a - \sigma_i$) driving dislocation motion played in microstructural evolution during plastic deformation cannot be distinguished. In such a case, Mohamed's model would miss some critical information about the physical mechanism(s) for microstructural evolution, which is unfavorable for us to design engineering materials with stable grain size via tuning their initial microstructures and/or processing parameters. Although tremendous efforts have been dedicated to investigating d_s in nontwinned FCC materials (Mohamed, 2003; Edalati and Horita, 2011), few studies have focused on how the grain size d evolves during room temperature (RT) plastic deformation in NT metals. In particular, the theoretical prediction of d_s in NT metals involving the thickness and fraction of nanotwins is still absent.

Apart from modeling their microstructural evolution in terms of underlying deformation mechanism(s), quantifying the time-dependent plasticity (*i.e.*, creep) of nanostructured metals at RT has been at the forefront of mechanics and materials research. For pure metals with submicron- and micron-sized grains, creep deformation is generally accomplished by the generation, motion and annihilation of dislocations, and the cell walls and subboundaries formed by dislocation groups play critical roles in their creep behavior (Orlová and Čadek, 1986; Kassner, 2009; Basirat et al., 2012; Zhao et al., 2015). In contrast, the behavior of dislocation groups emerged in large grain-sized metals likely disappears in NC metals, because there is insufficient space for collective dislocation interactions and the emitted dislocations from a GB can easily travel within the grain interior and become absorbed by the opposite GB, leaving a dislocation starved state (without dislocation accumulation) (Van Swygenhoven et al., 2006; Van Swygenhoven et al., 2002). The present authors have revealed that the Cu freestanding foils with a wide grain size-range of ~25–250 nm exhibit the change from a creep stress exponent of ~5 in bulk Cu to an exponent of ~3, which can be attributed to the lack of subgrains or dislocation substructures in UFG and NC Cu (Guo et al., 2013). This result is consistent well with the experiments of Hasegawa et al. (1972), which have clearly established that the dynamic internal stresses correlate well with the formation of subgrains and the change of creep stress exponent at steady state. In fact, the high (creep) strain rate sensitivity indicates that the short-range internal stress becomes more important during plastic deformation of nanostructured FCC metals, such as Cu (Guo et al., 2013) and Ni (Blum and Li, 2007). Abundant investigations (Chauhan and Mohamed, 2007; Barai and Weng, 2008; Choi et al., 2013; Gollapudi et al., 2010) on the creep behavior of NC metals have uncovered that GB-related processes like GB dislocation emission, GB sliding and GB diffusion are the underlying creep mechanisms, rendering that they exhibit several orders of magnitude enhancement of $\dot{\varepsilon}_{SC}$ in comparison with their CG counterparts. Although the creep deformation of NC FCC metals has been widely studied as mentioned above, the lack of quantitative information on the effect of nanotwins leads to uncertainty in understanding the creep behavior of their NT counterparts.

This study is thus motivated by two main objectives: one is to model the stable grain size d_s in NT metals (Ni) with high SFE during creep at RT, and the other is to quantify the strain rate $\dot{\varepsilon}_{SC}$ of NT Ni in terms of the effective stress σ_e, since σ_e is actually responsible for the creep deformation instead of the applied stress σ_a. This paper is organized as follows. After this introduction, which presents the background and outlines the motivations, a dislocation-based model to quantitatively capture d_s of NT Ni and to predict $\dot{\varepsilon}_{SC}$ in terms of σ_e is constructed in Section 2. In Section 3, the experimental details about the NT Ni sample preparation, the creep tests and the methods of internal stress measurement are clearly presented. In Section 4, (de) twinning-mediated grain growth/refinement and the size-dependent $\dot{\varepsilon}_{SC}$ under different σ_a are shown. In Section 5, the

predictive capacity of the theoretical model for the dislocation and grain growth/refinement dominated creep is verified by the observed d_s and $\dot{\varepsilon}_{SC}$, and the possible grain growth/refinement mechanisms are proposed in terms of dislocation-GB/TB interactions. Finally, the main findings are summarized together with the concluding remarks in Section 6.

2. Theoretical formalism

In order to interpret the stress and temperature effects on the creep behavior from the perspective of dislocations, two other stress characteristics are introduced except the applied stress (σ_a), *i.e.*, the internal stress (σ_i), characterizing the strain hardening of materials, and the effective stress (σ_e), acting on dislocations in their movements (Orlová et al., 1972). In fact, the applied stress σ_a is just opposed to the internal stress σ_i, which is thought to be a combination of two components: an athermal component σ_{ath} (*i.e.*, the long-range internal stress) and a thermal component σ_{th} (*i.e.*, the short-range internal stress), *i.e.*, $\sigma_i = \sigma_{ath} + \sigma_{th}(\dot{\varepsilon}, T)$ (Conrad, 1970; Kassner et al., 2013). The internal stress $\sigma_i = \sigma_{ath} + \sigma_{th}(\dot{\varepsilon}, T)$ is considered as a back stress that hinders dislocation motion in a specimen without considering its heterogeneous nature of the defect structure, while the effective stress $\sigma_e = \sigma_a - \sigma_i$ induces dislocation motion, which is closely correlated with the grain refinement or growth during creep.

2.1. Determination of internal stresses

To begin, the experimental methods and theoretical models are briefly introduced to estimate the internal stress σ_i. There are several available methods to determine the long-range internal stress σ_{ath}, as summarized in a review article by Conrad (1970). Here, we adopted two typical methods, *i.e.*, strain rate jump tests (Li, 1967) and fully relaxed stress tests (Kruml et al., 2008; Guiu and Pratt, 1964), both of which are widely used to measure σ_{ath} in nanostructured metals, such as NC Ni (Wang et al., 2006) and NT Cu (Lu et al., 2009b). The principles and validities of these two methods were discussed by Caillard and Martin (2003) in detail, and won't be presented here.

On the other hand, neglecting the small Peierls barrier in pure FCC metals, the internal stress can also be theoretically calculated, which is a combination of a component $\sigma_{i\text{-}\rho}$ that arises from the free dislocation density ρ (Orlová and Čadek, 1986) and a component $\sigma_{i\text{-}\theta}$ that arises from GBs with an average misorientation angle θ (Argon and Takeuchi, 1981). Due to the absence of the blocking effect of forest dislocations found in CG metals, the mobile dislocations can partly or fully insert into or pile up against GBs in UFG, even in NC metals (with grain size > 15 nm (Li et al., 2010), below which GB-mediated mechanism governs the plasticity) as a result of straining. This would exert a notable back stress $\sigma_{i\text{-}\rho}$ to hinder further dislocation motion, which has been uncovered by *in-situ* TEM observations in cyclically deformed UFG Al at RT (Mompiou et al., 2012). Simultaneously, these sessile or blocked dislocations under the applied stress would cause notable strain gradients (associated with geometrically necessary dislocations). This can result in elastic bending of a portion of a GB with the length of $\delta = d/2$ (d is the grain size) to accommodate for the incompatibility at GBs, which in turn triggers the generation of long-range internal stress $\sigma_{i\text{-}\theta}$ (Argon and Takeuchi, 1981). Therefore, in NC metals associated with homogenous microstructural features, given the contributions from the density of initial dislocations (ρ_0) and the misorientation angle between neighboring grains (θ), the long-range internal stress at RT can be approximately expressed as (Orlová and Čadek, 1986):

$$\sigma_i = \sigma_{i-\rho} + \sigma_{i-\theta} = \alpha M_T \mu b \sqrt{\rho_0} + \frac{\mu\theta}{8}\frac{y}{\delta}, \tag{1}$$

where α is the constant which equals typically ~0.1–0.5, M_T is the Taylor factor ~3.06, μ is the shear modulus, b is the magnitude of Burgers vector, $\frac{y}{\delta} = 0.8\frac{4(1-\upsilon)}{\pi}\left(\frac{\sigma_a\delta}{\mu b}\right)\left(\frac{b}{\theta\delta}\right)^{2/3}$ is an amplitude of bowing out of a polyhedral grain (Argon and Takeuchi, 1981), $\delta = d/2$ is the spacing between pinning points along the *tilt* boundary, and d is the grain size.

2.2. General considerations

Since the stable grain size d_s probably is associated with the chemical composition of GBs and the presence of impurities and/or small precipitates at GBs (TBs) can profoundly affect grain (twin) growth kinetics, we only focus on the “pure” nanostructured metals in this work. To rationalize the present dislocation-based model applicable to UFG and NC metals, we compare the characteristics of GBs and TBs, and make the following assumptions:

1) In real polycrystalline metals, a spread in available grain sizes and a spread in activation energies (dictated by a distribution in GB structures) are expected. For grain size distribution, the number of grains with various diameters in NC metals can usually be well represented by a *lognormal distribution function* (Zhu et al., 2005). For simplicity, we only use the arithmetic average grain size determined from the *lognormal distribution function* rather than the size-distribution in this dislocation-based model. The same treatment is applied to the estimation of twin thickness λ. Accordingly, the model assumes discrete values for the GB self-diffusion (activation energy) associated with a peculiar misorientation angle and for the grain size of the material.

2) In the present NT Ni foils, the model assumes that GBs possess scale-independent nature (*e.g.*, structure and width) (Carlton and Ferreira, 2007), and belong to the low-angle *tilt* GBs for the sake of simplicity during subsequent theoretical calculations. In fact, several studies have revealed that the structure and width of GBs are essentially the same for NC and CG materials (Kumar et al., 2003; Van Swygenhoven et al., 2000).
3) Because GBs become penetrable in UFG and NC metals (Mompiou et al., 2012), the gliding dislocation is near or (partly/fully) inserts into a GB, strain gradients (associated with geometrically necessary dislocations) arise to trigger the elastic deformation of GBs to accommodate for the incompatibility at GBs. This model assumes that a portion of the *tilt* GB would be flexed out between pinning points under the applied stress, similar to the case of sub-boundary flexure under stress (Argon and Takeuchi, 1981). This scenario corresponds to the micro-flexible boundary condition, which is in-between micro-clamped and micro-free boundary conditions (Ekh et al., 2011; Gurtin, 2008).
4) Somewhat different from GBs, this model assumes that the defective coherent TBs (CTBs), also serving as dislocation sources, are penetrable so that dislocations can transmit them finally, but the possible stress filed effect caused by these transmitting dislocations on the internal stress can be neglected. Recent *in-situ* TEM observations (Lu et al., 2015) have uncovered that only a small fraction of dislocations nucleated from the steps on CTBs would transmit these defective CTBs, and most of them nucleated from the TB-GB junctions would glide along these TBs in the present strength softening regime with λ less than ~40 nm (Li et al., 2015). The initial (source) dislocations inside the nanotwins merely contribute to the athermal stress which stems from the density of initial dislocations (ρ_0), *i.e.*, $\sigma_{i\text{-}\rho}$.

Next, we will construct a dislocation-based model to predict d_s of nanostructured NT metals (*e.g.*, Ni and Cu) with the fraction of twinned grains f and subsequently to quantify $\dot{\varepsilon}_{SC}$.

2.3. A model for dislocation and grain growth dominated creep

As mentioned earlier, Mohamed (2003) proposed a dislocation-based model to predict the stable grain size d_s, inspired by high similarities between d_s obtained by plastic deformation and $\dot{\varepsilon}_{SC}$ associated with dislocation creep, both of which are reached when a dynamic balance occurs between: (i) hardening arisen from dislocation multiplication and interaction, and (ii) recovery caused by dislocation annihilation and rearrangement. Previous study (Chauhan and Mohamed, 2007) has uncovered that the grain size increases to a saturation value of d_s in bulk NC Ni when $\dot{\varepsilon}_{SC}$ is reached during creep at RT. This likely implies that both d_s and $\dot{\varepsilon}_{SC}$ during creep share the common physical mechanism in terms of the competition between σ_i and σ_e, characterized by the stress ratio $\eta_{Stress} = \sigma_e/\sigma_i$. However, in Mohamed's model, dislocations are mainly generated from bulk sources, unlike the cases of UFG and NC metals, in which dislocations are emitted from GBs and/or TBs (Lu et al., 2009a; Li et al., 2010). That is to say, grain refinement or grain growth in UFG and NC metals can be dominantly attributed to the GB-related dislocation activities. In a NC metal with the grain size of d, at steady state, the density of mobile dislocations emitted from GBs, ρ_m, can be taken to be (Li and Chou, 1970)

$$\rho_m = \frac{\varepsilon}{bd} = \frac{3\omega}{d}, \tag{2}$$

where ω represents the total length of emitted dislocations from the unit area of GB, corresponding to the linear atomic density of the dislocation line (Carlton and Ferreira, 2007).

Based on the spirit of Argon and Takeuchi (1981), if assuming that only parts of mobile dislocations which are incompletely attached to boundaries (*i.e.*, GBs and TBs) would serve as sources in nanostructured NT metals during creep, and that the more widely a dislocation is extended, the less probable it acts as source for an appropriate segment (Argon and Takeuchi, 1981), the source density per unit projected area can be then expressed as:

$$M \approx f\rho_m\left(\frac{b}{x}\right)\left(\frac{d}{\lambda}\right) + (1-f)\rho_m\left(\frac{b}{x}\right), \tag{3}$$

where f is the fraction of twinned grains, λ is the twin thickness, x denotes the equilibrium extension of the SF on an edge dislocation, and can be given by Argon and Takeuchi (1981):

$$\frac{x}{b} = \frac{(2+\upsilon)}{24\pi(1-\upsilon)}\left(\frac{\mu b}{\gamma}\right), \tag{4}$$

where υ is Poisson's ratio, and γ is the SFE. It is well known that the plastic strain ε and the corresponding strain rate $\dot{\varepsilon}$ can be respectively written as (Mohamed, 2003; Hirth and Lothe, 1982):

$$\varepsilon = N_V bA, \tag{5}$$

and

$$\dot{\varepsilon} = \frac{d\varepsilon}{dt} = \rho b \bar{v}, \tag{6}$$

where A is the average area of slip plane swept by a dislocation, which is on the order of L^2, $L \approx d/2$ is the length of dislocation pile-up, $\bar{v}$ is the average dislocation velocity, N_V is the number of dislocations per unit volume, and can be derived as:

$$N_V = M_V N \approx \frac{9K\pi\omega}{2M_T b}\left(\frac{\sigma_e}{\mu}\right)\left(\frac{b}{x}\right)\left[\frac{f}{\lambda} + \frac{(1-f)}{d}\right], \tag{7}$$

where $M_V = \frac{M\pi d^2/2}{\pi d^3/6} \approx \frac{3}{d}\rho_m\left(\frac{b}{x}\right)\left[f\left(\frac{d}{\lambda}\right) + (1-f)\right]$ is the dislocation source density per unit volume, N is the number of dislocations in each group, K is a constant ($K = 1$ for screw dislocations and $K = (1-\upsilon)$ for edge dislocations).

In fact, the premise of reaching the stable grain size d_s is that the grain size-increase rate $(\delta d/\delta t)^+$ balances the grain size-decrease rate $(\delta d/\delta t)^-$, *i.e.*, $(\delta d/\delta t)^+ = (\delta d/\delta t)^-$. Following the treatment of Friedel (1964) and taking the dislocation climb velocity $v_c = v_0\left(\frac{\sigma_e}{\mu}\right)$, the former, assumed to be in proportion to the recovery rate, can be expressed as (Hirth and Lothe, 1982; Mohamed, 2003):

$$(\delta d/\delta t)^+ = C_1\frac{v_c}{w}b = C_1 v_0\left(\frac{\sigma_e}{\mu}\right)\theta, \tag{8}$$

where C_1 is a stress-dependent coefficient, reflecting the rate of grain growth, $w = b/\theta$ is the climb distance of two edge dislocations and v_0 is the unit velocity of an extended edge dislocation, yielding (Argon and Takeuchi, 1981)

$$v_0 = 2\left(\frac{24\pi(1-\upsilon)}{2+\upsilon}\right)^2\left(\frac{D}{b}\right)\left(\frac{\mu\Omega}{kT}\right)\left(\frac{\gamma}{\mu b}\right)^2 c_j, \tag{9}$$

where $D = D_V + D_{GB} + a_c\rho D_P$ represents the effective diffusion coefficient, D_V, D_{GB} and D_P are coefficients for self-diffusion, GB diffusion and dislocation pipe diffusion, respectively, a_c refers to the cross-sectional area of the dislocation core associated with rapid diffusion (Mohamed, 2003), Ω is the atomic volume, $c_j = c_0\mathbf{exp}\left(\frac{\sigma_e bh\zeta}{M_T kT}\right)$ is the jog concentration along the dislocation (Hirth and Lothe, 1982), c_0 is the thermal equilibrium concentration of jogs, h is the distance climbed by the dislocation and ζ is the spacing of obstacles. While the latter is supposed to be proportional to the energy caused by the effective stress during plastic deformation, and it can be written as (Mohamed, 2003):

$$(\delta d/\delta t)^- = \left(\frac{\delta d}{\delta\varepsilon}\right)\left(\frac{\delta\varepsilon}{\delta t}\right) = C_2 b\frac{\sigma_e}{\mu}\varepsilon\dot{\varepsilon} = C_2\frac{27K\omega^2\theta^2 b v_0}{4M_T(1-\upsilon)}\left(\frac{\sigma_e}{\mu}\right)^2\left(\frac{b}{x}\right)\left[f\left(\frac{d^2}{\lambda}\right) + (1-f)d\right], \tag{10}$$

where C_2 is a stress-dependent coefficient, reflecting the rate of grain refinement. Considering the balanced condition, one can obtain the stable grain size d_s as follows:

$$\frac{d_s}{b} = \frac{\sqrt{(1-f)^2 + C\frac{f}{\lambda}\frac{2M_T(2+\upsilon)}{81K\omega^2\pi b\theta}\left(\frac{\mu}{\sigma_e}\right)\left(\frac{\mu b}{\gamma}\right)}}{2f}\frac{\lambda}{b} - \frac{1-f}{2f}\frac{\lambda}{b} \quad \text{for } (0 < f \le 1), \tag{11a}$$

and

$$\frac{d_s}{b} = C\left[\frac{(2+\upsilon)M_T}{162\pi K b^2\omega^2\theta}\right]\left(\frac{\mu b}{\gamma}\right)\left(\frac{\mu}{\sigma_e}\right) \quad \text{for } (f = 0), \tag{11b}$$

where C is a stress-dependent coefficient in-between the growth rate C_1 and the refinement rate C_2, and a useful representation of the coefficient C as a function of σ_e, consisting of C_1 and C_2 below and above the critical stress σ_i, respectively, is $C = \frac{C_1+C_2}{2} - \frac{C_1-C_2}{2}\mathrm{erf}\left(\frac{\sigma_e-\sigma_i}{\Delta}\right)$, Δ is a measure of the extent of the transition region (Kim et al., 2011). Indeed, it is found from Eq. (11) that the stable microstructure characteristics are intimately related to the steady-state values of applied, internal and effective stresses.

As documented by Chauhan and Mohamed (2007) and Gollapudi et al. (2010), the results of the structure observations correspond well to the macroscopic creep data, *i.e.*, there is no significant grain growth or refinement once the steady-state creep stage is reached. During creep, the rate of increase in mobile dislocations from M sources per unit projected area can be written as (Argon and Takeuchi, 1981):

$$\dot{\rho}_m^+ = \frac{M}{\chi} v_c = \frac{M v_0}{\beta b}\left(\frac{\sigma_e}{\mu}\right)^2, \tag{12}$$

where $\chi \approx \beta\mu b/\sigma_e$ is the climb distance in a boundary, and $\beta \approx 0$–0.1 is a dimensionless coefficient. On the other hand, by combining with the geometrical relation of mobile dislocation density $\rho_m = 1/(lw)$, one can acquire the rate of annihilation of mobile dislocations (Argon and Takeuchi, 1981):

$$\dot{\rho}_m^- = -\frac{\rho_m}{t_a} = -\frac{2v_0 b\rho_m}{\pi(1-\upsilon)w^2} = -\frac{2v_0 b}{\pi(1-\upsilon)}\left(\frac{l}{w}\right)\rho_m^2. \tag{13}$$

Via equating Eq. (12) to Eq. (13), ρ_m at steady-state creep is written as

$$\rho_m = \frac{12\pi^2(1-\upsilon)^2}{(2+\upsilon)\beta b^2}\left(\frac{\gamma}{\mu b}\right)\left(\frac{\sigma_e}{\mu}\right)^2\left(\frac{w}{l}\right)\left[f\left(\frac{d}{\bar{\lambda}}\right) + (1-f)\right], \tag{14}$$

where l is the mean free path of dislocations, scaling with d. Now, $\dot{\varepsilon}_{SC}$ can be obtained

$$\dot{\varepsilon}_{SC} = \rho_m b\bar{v} = \frac{2}{\beta}\left(\frac{24\pi(1-\upsilon)}{(2+\upsilon)}\right)^3\left(\frac{\sigma_e}{\mu}\right)^2\left(\frac{\mu\Omega}{kT}\right)\left(\frac{D\theta}{b^2}\right)\left(\frac{\gamma}{\mu b}\right)^3\left[f\left(\frac{d}{\bar{\lambda}}\right) + (1-f)\right]c_j. \tag{15}$$

It is found from Eq. (15) that $\dot{\varepsilon}_{SC}$ is closely related to the effective stress σ_e and material parameters including μ, Ω, D, γ, θ, d and λ.

At the same time, a dynamic equilibrium emerges between work hardening and recovery softening in the steady-state creep stage, leading to the time-independent internal stress (Ahlquist et al., 1970). The evolution of dislocation density determined by the competition between dislocation generation and annihilation can be expressed as (Kocks et al., 1975):

$$\frac{\mathrm{d}\rho}{\mathrm{d}t} = \frac{\mathrm{d}\rho^+}{\mathrm{d}t} - \frac{\mathrm{d}\rho^-}{\mathrm{d}t} = \frac{\dot{\varepsilon}}{lb} - \frac{\rho(t)}{t_a}, \tag{16}$$

where $t_a = \frac{\pi(1-\nu)}{2bv_0}w^2$ is the time for mutual annihilation of two edge dislocations within a distance w ($= b/\theta$) (Argon and Takeuchi, 1981), v_0 is the unit velocity mentioned above. Accordingly, the solution of the differential Eq. (16) is:

$$\rho(t) = \frac{\dot{\varepsilon}t_a}{db} + \left(\rho_0 - \frac{\dot{\varepsilon}t_a}{db}\right)e^{-t/t_a}, \tag{17}$$

where ρ_0 is the initial dislocation density when entering the creep process, and can be determined from the initial strain at the onset of primary creep ε_0 via the relation: $\varepsilon_0 = \rho_0 bl$. Also, we assume that the internal stress caused by misorientation angle between neighboring grains always exists and is almost a constant, considering that GBs do not disappear during creep. Therefore, the evolution of total internal stress with time in creep can be simply expressed as:

$$\sigma_i(t) = \sigma_{i0} - \alpha M_T \mu b\sqrt{\rho_0} + \alpha M_T \mu b\left[\left(\frac{\dot{\varepsilon}t_a}{db}\right) + \left(\rho_0 - \frac{\dot{\varepsilon}t_a}{db}\right)e^{-t/t_a}\right]^{1/2}. \tag{18}$$

It should be noted that this model is based on the ordinary dislocation mechanism, which in general control the plasticity above a critical size of ~15 nm, below which the microstructure and mechanical response (*e.g.*, the so-called inverse Hall–Petch relation) of metals are mainly controlled by the GB-mediated processes, such as GB sliding, grain rotation and GB diffusion (Carlton and Ferreira, 2007).

3. Experimental methods

3.1. Material preparation

High purity NT Ni foils (~99.999 wt.%) with thickness of 10 microns (the initial grain size d_0 ~ 84 nm and 120 nm, respectively) were synthesized on a stainless steel substrate by a pulse electrodeposition (PED) technique in an electrolyte of nickel sulfate without any grain refiners, which aims at reducing/eliminating the introduction of impurities into samples. By tuning the electrodeposition parameters, such as the cathode current density and deposition time *etc*, samples with different initial average grain sizes (d), number fractions of twinned grains (f, here a twinned grain refers to a grain containing at least one TB) and almost constant average twin thickness ($\lambda \sim 38 \pm 2$ nm) could be prepared experimentally: NT Ni with $d_0 \sim 84$ nm and $f \sim 60\%$ is obtained with a peak current density of 5 A dm^{-2}, $d_0 \sim 120$ nm NT Ni with $f \sim 67\%$ is prepared with a peak current density of 6.25 A dm^{-2}. The preparation process is described in detail in our previous work (Li et al., 2015). Note that, the statistical grain size distributions as well as the twin thickness distributions of both samples are fitted by a *lognormal*

distribution function, as shown in Fig. 1, following the procedure adopted by Zhu et al. (2005). The number fraction of the twinned grains is defined as the number of twinned grains per unit area divided by the total number of grains per unit area. Microstructural features of the NT Ni foils before and after creep were characterized by using a JEOL-2010F high resolution transmission electron microscope (HRTEM) operated at 200 kV, and the elemental composition (or purity) analysis of the specimens is identified by energy dispersive X-ray (EDX).

3.2. Creep experiments

Creep tests of free-standing NT Ni foils with a gage section of 20 mm long and 3 mm wide were carried out at RT by using a MTS-Tytron 250 testing machine. These samples with different grain sizes were first loaded under different loading rates (50 mN s^{-1}, 5 mN s^{-1} and 0.5 mN s^{-1}), and were then respectively held at constant applied stresses ranging from 400 to 900 MPa for a given period of time. More than three repeated creep tests were carried out under each constant applied stress.

3.3. Measurement of internal stress

To measure the internal stress of NT Ni samples and compare with the calculated results, uniaxial tensile strain rate jump experiments and full stress relaxation tests were also conducted on the MTS-Tytron 250 at RT. The strain rate change experiments were carried out by immediately increasing the strain rate at a certain plastic strain during strain rate-controlled tensile tests, with strain rate jumping from $\dot{\varepsilon}_1 = 1 \times 10^{-5}\ s^{-1}$ to $\dot{\varepsilon}_2 = 2 \times 10^{-5}\ s^{-1}$ and then to $\dot{\varepsilon}_3 = 4 \times 10^{-5}\ s^{-1}$ to meet the premise of $\dot{\varepsilon}_2/\dot{\varepsilon}_1 = \dot{\varepsilon}_3/\dot{\varepsilon}_2$. By assuming that both the internal stress and the ratio of mobile dislocation density remain unchanged during the change in strain rate, the internal stresses can be calculated via the formula: $\sigma_i = (\sigma_1\sigma_3 - \sigma_2^2)/(\sigma_1 + \sigma_3) - 2\sigma_2$, where σ_1, σ_2 and σ_3 are the corresponding stresses at strain rates of $\dot{\varepsilon}_1$, $\dot{\varepsilon}_2$ and $\dot{\varepsilon}_3$, respectively (Li, 1967). For full stress relaxation experiments, the NT Ni samples were initially stretched to the total (elastic + plastic) strain

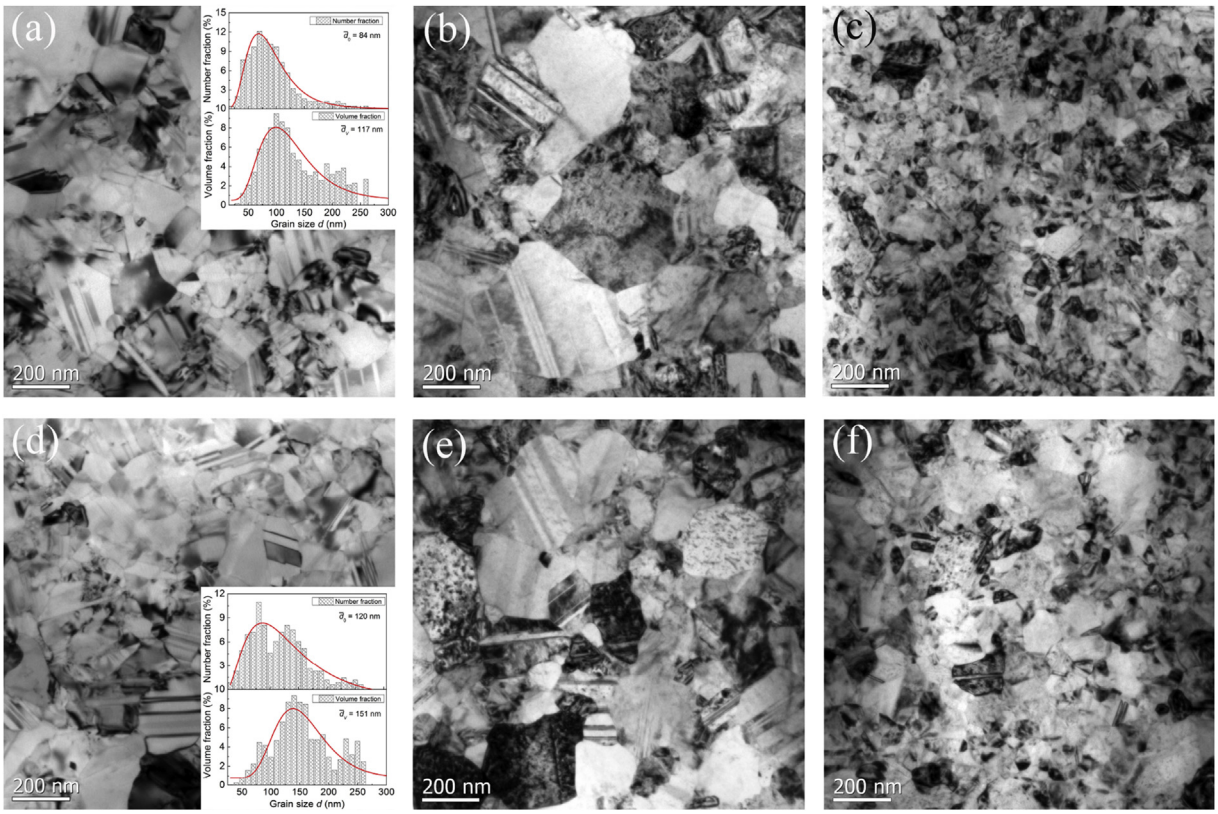

Fig. 1. TEM bright field images of 84 nm and 120 nm grain size NT Ni before and after creep under a loading rate of 50 mN·s^{-1} with the applied stress σ_a~400 MPa and 900 MPa. It is obvious that the microstructural characteristics exhibit significant changes compared with those of as-deposited state, such as grain growth, grain refinement, twin fraction increase and twin thickness decrease. (a, b, c) as-deposited, 400 MPa and 900 MPa of 84 nm, respectively; (d, e, f) as-deposited, 400 MPa and 900 MPa of 120 nm, respectively. The inset in (a) and (d) are the corresponding statistical distributions of grain size for as-deposited NT Ni samples. The curves are lognormal regression curves and the arithmetic average grain sizes from the statistical number fractions are adopted in the study.

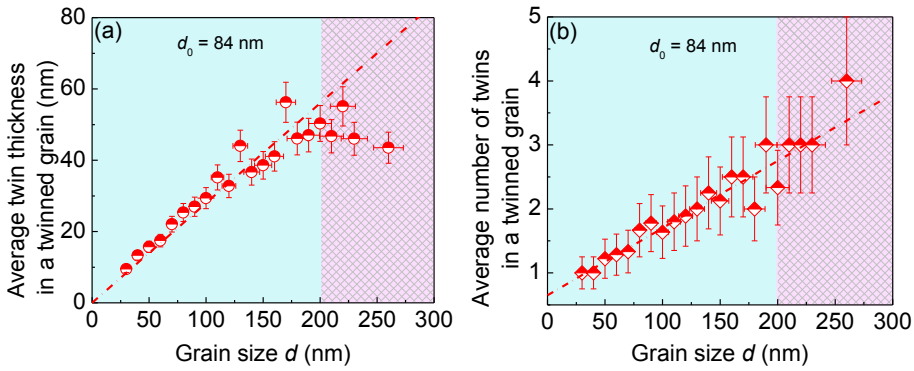

Fig. 2. Average twin thickness (a) and average number of twins (b) in a twinned grain plotted as a function of grain size d for 84 nm NT Ni. Due to the lower number fraction of larger grains (grain size d > 200 nm), the corresponding statistical results deviate from the linear relationship (the parts of sparse grid).

of 0.6% in a displacement controlled mode at a strain rate of 1×10^{-3} s^{-1}. Then the cross-head was ceased and the decrease in stress as a function of time was automatically recorded. The internal stress, corresponding to the stress plateau, can be directly read from the stress–time curve. It should be noted that the stress, in this test method, must be fully relaxed to yield σ_{ath}, as pointed out by Conrad (1970).

4. Results

4.1. Microstructural evolution of NT Ni during creep

Fig. 1 shows the representative plan-view TEM images of 84 nm and 120 nm grain size NT Ni before and after creep at a loading rate of 50 mN s^{-1} with the applied stress levels of 400 MPa and 900 MPa. For the as-deposited NT Ni foils, it is obvious that they have a wide grain size distribution spanning from 20 to 300 nm, as seen from the statistical results in Fig. 1. By fitting the statistical grain size distributions of both samples using the *lognormal distribution function*, one can obtain the arithmetic average grain size of ~84 and ~120 nm for these two samples, respectively. Similarly, one can get the arithmetic average twin thickness of ~36 and 40 nm for 84 and 120 nm NT Ni, respectively. Meanwhile, we show the average twin thickness in a twinned grain as a function of d in Fig. 2(a), and found that there is a linear scaling behavior between grain size and twin thickness (except for the case of larger sized grains (>200 nm) due to their lower fractions) in the present NT Ni system, *i.e.*, the ratio of d/λ is constant (~3.5 for 84 nm NT Ni and ~3.6 for 120 nm NT Ni). Also, the average number of twins in a twinned grain as a function of d is presented in Fig. 2(b). It seems that these nontwinned grains are always small grains with $d < 50$ nm, especially for the grains less than 30 nm. In this regard, the characteristic size, *i.e.*, minimum $\{d, \lambda\}$, distributes in a narrow size-range spanning from ~20 to 60 nm, implying that the deformation mechanism is based on the partials emitted from GBs and TBs in the present NT Ni (Li et al., 2015). Through detailed HRTEM analysis, stacking faults (SFs) and secondary twins were rarely observed between primary TBs.

It is striking to find that microstructural characteristics exhibit significant changes compared with those of the as-deposited state, such as grain growth or refinement, twin fraction increase and twin thickness decrease. The resultant grain sizes of NT Ni foils loaded at different loading rates to different stress levels spanning from 400 to 900 MPa are presented in Fig. 3, which can be divided into three regions, *i.e.*, R_I, R_{II} and R_{III}, as detailed below.

1) In R_I for low stress levels, one can find that the grain sizes for both 84 nm and 120 nm NT Ni remarkably increase to d_s ~220 ± 20 nm at the steady-state creep stage. Similarly, grain coarsening process at ambient temperature has been observed in deformed NT Cu with average grain size of ~25 nm (Brons et al., 2013) and fatigued NC Au with average grain size of ~19 nm (Luo et al., 2014), both of which with medium level of SFE. Importantly, this saturation size of ~220 ± 20 nm are nearly independent of the applied stresses and strain rates in the present testing conditions, implying that the long-range internal stress σ_{ath} plays a critical role in grain growth. Also, there is an obvious increase in the fraction of twinned grains f to ~85% in these NT Ni foils with different d_0 at the steady-state creep stage accompanied with somewhat reduced twin thickness λ to a stable size of λ_s ~ 32 ± 2 nm, compared to their as-deposited siblings (λ ~ 38 ± 2 nm) (see Fig. 3). It seems that grain growth is likely related to (de)twinning processes in NT metals.
2) In R_{II} for the medium stress level (~800 MPa), by contrast, both NT Ni samples exhibit quite stable grain sizes, comparable with those of the as-deposited state. However, these NT Ni samples show an increase in f to ~77% and marked decrease in λ to λ_s ~ 9 nm, almost identical to the corresponding values under the high stress level.
3) In R_{III} for high stress levels, however, both the 84 nm and 120 nm grain size NT Ni foils show significant grain refinement, associated with a notable reduction in λ, as seen in Fig. 3. For example, the grain size of 84 nm NT Ni samples held under σ_a ~ 900 MPa decreases from 84 to 50 nm, associated with a notable reduction in λ from 35 to λ_s ~7 nm and with the total fraction of twinned grains of ~77%. This is contrary to the findings at the low stress levels, implying the effective stress σ_e likely becomes more important in grain refinement of NT Ni.

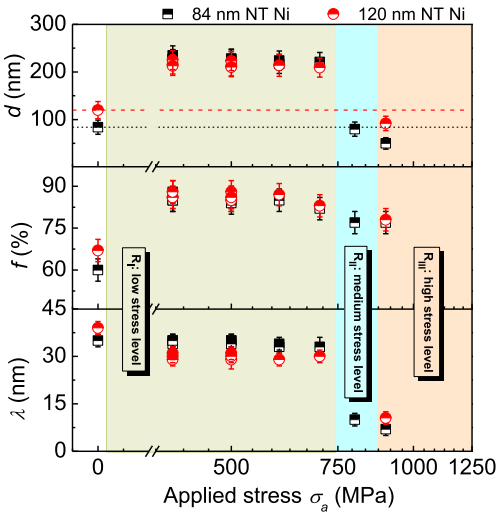

Fig. 3. The evolution of microstructural characteristics (grain size d, fraction of twinned grains f and twin thickness λ) for NT Ni before and after creep loaded at different loading rates and held under different stress levels spanning from 400 to 900 MPa.

Taken together, the present experimental findings unambiguously demonstrate that stress levels can notably affect the evolution of microstructures, in particular the characteristic sizes of grains and nanotwins. The microstructural evolution seems to be closely correlated with the (de)twinning process in the present NT Ni. Next, through HRTEM observations, we provide atomic evidence of (de)twinning-mediated grain growth and grain refinement in NT Ni, respectively.

Fig. 4 shows the atomic evidence of twinning-mediated grain growth in NT Ni, essentially being the consequence of nanotwin-assisted GB dissociation and local grain coarsening, which has been observed in NC Au (Luo et al., 2014) and NC Cu (Hu et al., 2016). Fig. 4(a) shows the configurations of a large grain (G1) and two small grains (G2 and G3) in a deformed 84 nm Ni sample with typical multi-twins. Some nanotwins changed the local orientation of G1 to the same orientation as G2. For this reason, some parts of G1 were transformed into G2 through such multiple formation of nanotwins, rendering some localized segments of GB between G1 and G2 (marked by red asterisks) to dissociate gradually (see Fig. 4(b) and (c)). This is because there is enough time to sustain the continuous formation of nanotwins in neighboring grains (*i.e.*, G1 and G2) during creep, and simultaneously these twinning partials would frequently hit on GBs. This process not only stimulates the emission of partials from GBs, but also facilitates the dissociation of GBs and local change of orientation. Therefore, the formation of nanotwins likely leads to a fact that some local parts of the high-angle GB are transformed into several new low-angle GB segments. Especially, these parts of the undissociated (high-angle) GBs are generally energetically higher and become much more mobile than the whole GB under the applied stress (Upmanyu et al., 2002; Winning et al., 2002). These recurrent interactions between partials/twins and GBs would facilitate the two adjacent nanograins to gradually coalesce into one larger grain with nanotwins. Such a nanotwin-assisted grain growth is more prone to occur in the grains with low-angle GBs, because the misorientation angle between two adjacent nanograins is easier to diminish via absorbing dislocations. It should be pointed out that there is a great possibility for the present mechanism to occur in G1/G2 with different mutual misorientation (θ) through the rotation around four typical low-index symmetric axes <*hkl*>, in particular for θ<*111*> (θ = 0–10°, 50–70°, 110–130° and 170–180°) and θ<*110*> (θ = 0–10°, 29–48.9°, 60.6–80.5°, 99.5–119.4°, 131.1–151° and 170–180°), as predicted by Luo et al. (2014). In parallel, the reduction in λ displayed in Fig. 3 after creep suggests that the detwinning process switches on. Twin steps at TBs are frequently observed in deformed NT Ni foils (not shown here), similar to that in our uniaxially stretched NT Ni reported before (Li et al., 2015). This finding likely implies that thinning of a nanotwin via the movement of steps along TBs is the first stage of detwinning and would become an operative mechanism for grain growth.

Fig. 5 provides the typical TEM images of grain refinement via the detwinning process caused by interactions between partial dislocations and primary TBs. Examples of the interactions are shown in Fig. 5(b) and (c). It is found that at the intersection of the primary and secondary twins, the atomic arrangement is distorted by dislocations, as verified by the fast Fourier transforms (FFTs) analysis of R3 in Fig. 5(b). The existence of SFs in the lower part of the primary twin (on the right of the secondary twin) signifies the gliding of Shockley partials produced via dislocation-TB reactions, which has been systematically analyzed by Zhu et al. (2011). These partials glide parallel to CTB, leading to detwinning of the primary twin (Cao et al., 2015). A similar phenomenon was observed in the twins crossed region of R4 in Fig. 5(c). Additionally, one can observe in Fig. 5(c) that two Shockley partials in the opposite directions are emitted from CTBs, consistent with the *in-situ* TEM observations in NT Cu (Lu et al., 2015). This supports our previous assumption that the (defective) CTBs become available dislocation sources in NT Ni samples. Actually, this is the first step to form secondary twins in-between primary twins to realize detwinning via the interaction of secondary twins and primary TBs. As further straining, these partials trigger the formation of SFs, even nanotwins, which would interact with primary twins to produce abundance of sessile dislocations,

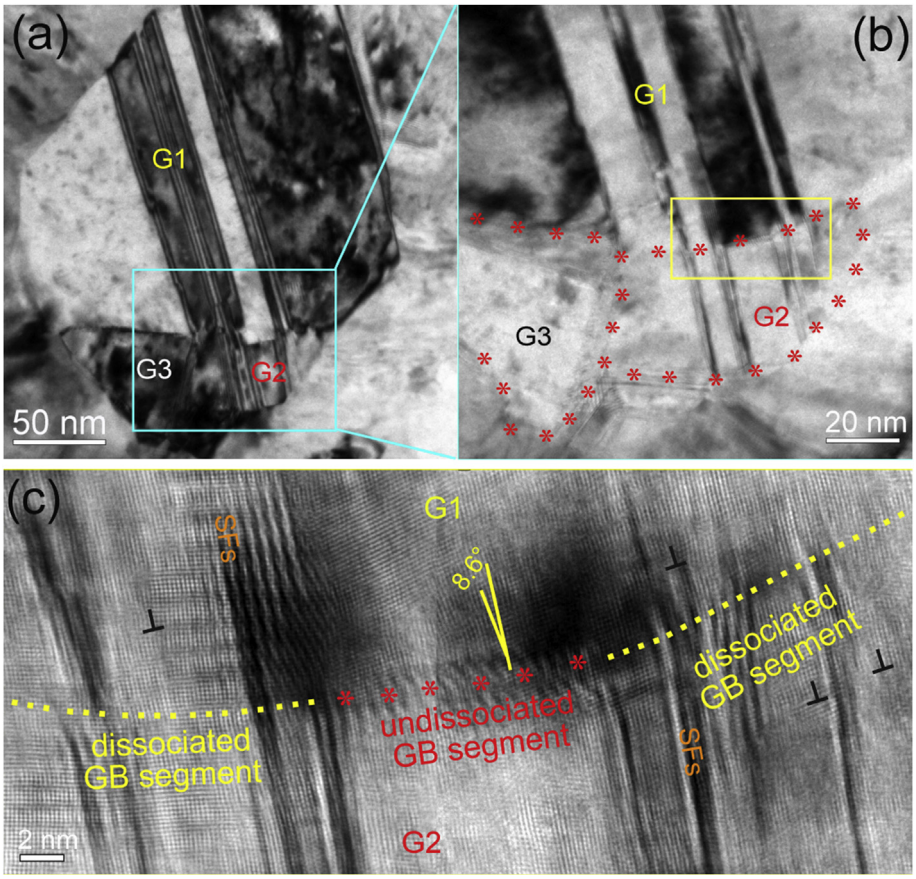

Fig. 4. Twining-mediated grain growth. (a) Typical TEM image of NT Ni after creep; (b) a close observation of the neighboring grains (G1, G2 and G3) in blue rectangle region in (a); (c) HRTEM images of twin-GB interactions in yellow rectangle region in (b) showing GB dissociation induced by twinning. The red asterisks indicate GB, the yellow dashed lines denote the dissociated GB segments, and the symbol "⊥" represents the dislocation. SFs mark the stacking faults. G1 and G2 have a small misorientation of ~8.3°. (For interpretation of the references to colour in this figure legend, the reader is referred to the web version of this article.)

thereby rendering CTBs to lose their coherency and transform into conventional GBs, eventually to achieve grain refinement (Cao et al., 2015).

4.2. Steady-state creep strain rate and internal stress

Fig. 6(a) presents the creep strain rate of d_0 ~ 84 nm NT Ni as a function of holding time loaded at a loading rate of 50 mN s^{-1} and held at different applied stresses. It is found that the creep strain rate notably decreases with increasing holding time and reaches a constant when entering into the steady-state creep regime. The variations in $\dot{\varepsilon}_{SC}$ with σ_a at different loading rates are presented in Fig. 6(b), from which one can see that at a given σ_a, a faster loading rate renders a slower $\dot{\varepsilon}_{SC}$. Moreover, in the present NT Ni foils, $\dot{\varepsilon}_{SC}$ decreases with reducing d at a relatively low stress level, while at a high stress level, $\dot{\varepsilon}_{SC}$ exhibits an increased trend with decreasing d (see Fig. 6(b)), which is mainly attributed to the transition from grain growth reduced $\dot{\varepsilon}_{SC}$ to grain refinement enhanced $\dot{\varepsilon}_{SC}$ with increasing σ_a. The detailed interpretation is in a separate paper and will not be discussed here.

To fundamentally understand the competition between internal stress σ_i and effective stress σ_e as well as their important roles played in the creep behavior at RT and other plastic deformation processes, such as severe plastic deformation and mechanical fatigue, both strain rate jump tests (see Fig. 7(a)) and stress relaxation tests (see Fig. 7(b)) are carried out to determine σ_i for our present NT Ni. The values of σ_i obtained from jump tests are ~380 MPa for d_0 ~84 nm and ~385 MPa for d_0 ~120 nm, respectively. Similarly, the corresponding curve of stress relaxation for d_0 ~84 nm NT Ni when the uniaxial tension is interrupted is shown in Fig. 7(b), from which σ_i ~380 MPa can be directly read, the same as that calculated from jump tests. These experimentally desired values agree well with the theoretical ones calculated via Eq. (1) by taking the following parameters: $\upsilon = 0.31$, $\mu = 94.7$ GPa (Hirth and Lothe, 1982), $b = 0.249$ nm, $\theta = 10°$ (for low-angle GBs (Luo et al., 2014)). Note that, in the strain rate jump tests, it appears that the d_0 ~84 nm NT Ni exhibits lower flow stress compared to that of d_0 ~120 nm NT

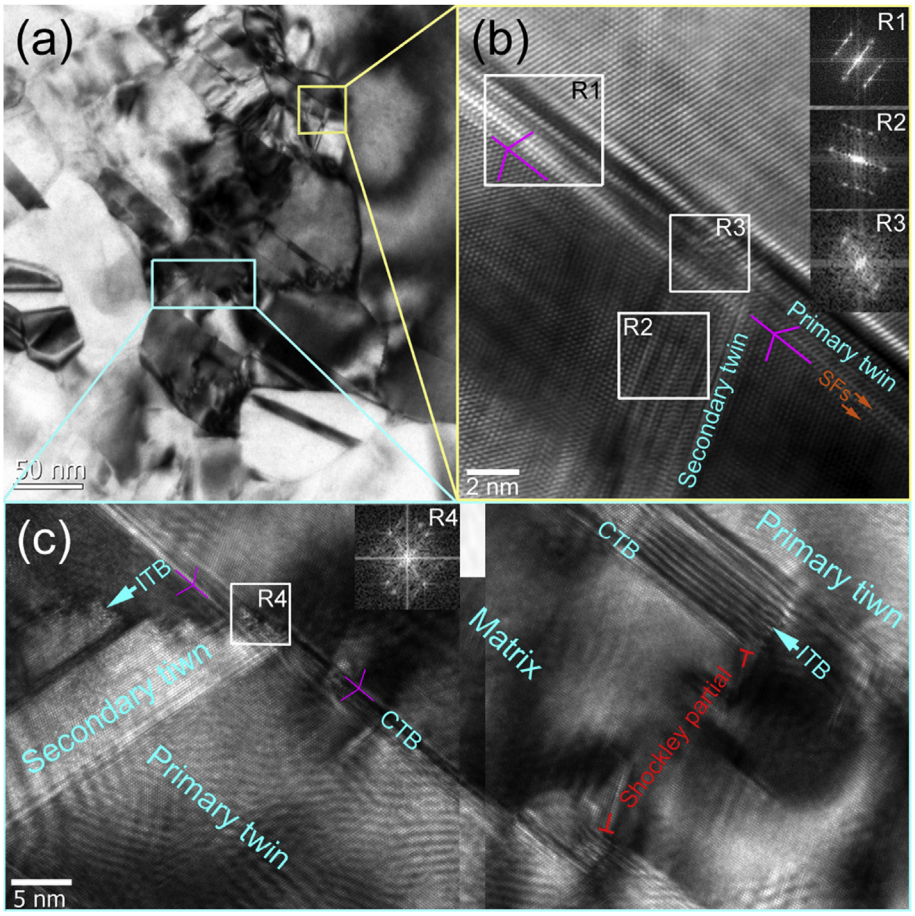

Fig. 5. Detwinning-associated grain refinement. (a) A typical TEM micrograph showing the GB formation via interactions between secondary twin and primary TB; (b) and (c) are the examples of interactions of primary and secondary twins in the yellow and blue rectangle region in (a), respectively. The inset in (b) and (c) are the corresponding fast Fourier transforms (FFTs) analysis of R1 and R2, showing the twin relationship, and R3 and R4, indicating the formation of local distorted regions (or the initial GBs). The violet lines indicate twin relationship, and the symbol "⊥" denotes the partial dislocation. The existence of SFs in the lower part of the primary twin (on the right of the secondary twin) signifies the emission of Shockley partials from TBs. (ITB: incoherent twin boundary, CTB: coherent twin boundary, SFs: stacking faults). (For interpretation of the references to colour in this figure legend, the reader is referred to the web version of this article.)

sample. This strength softening behavior is caused by the dislocation nucleation-controlled mechanism in these NT Ni foils with $\lambda < 40$ nm, similar to the case of NT Cu with $\lambda < 15$ nm (Li et al., 2010). More discussion can be referred to our previous work (Li et al., 2015) and won't be presented here.

5. Discussion

5.1. A new criterion for the stable grain size: stress ratio of effective to internal stress

In Section 2, we have established a dislocation model to quantitatively elucidate d_s of nanostructured metals, see Eq. (11). The stable grain size d_s as a function of the effective stress σ_e predicted from Eq. (11) for NT Ni with different f and with different λ are plotted in Fig. 8(a) and (b), respectively. It appears that d_s in either twinned or nontwinned metals monotonically decreases with increasing σ_e (see Fig. 8(a)). Moreover, it is also uncovered that Eq. (11a) broadly captures d_s of the present NT Ni within the scatter, as indicated by the red dashed line in Fig. 8(a) for the best fitting of the data with $2\sigma_e = \sigma_a$ (or stress ratio $\eta_{Stress} = \sigma_e/\sigma_i = 1$) and $f = 0.6$. This prediction also agrees well with our previous results obtained from the uniaxial tensile tests on the same NT Ni samples with $f = 0.6$ (Li et al., 2015), see Fig. 8(a). In addition, it provides a reasonable explanation why the HPT method more effectively refines grains (d_s ~240 nm for pure Ni (Edalati and Horita, 2011)) than ECAP (d_s ~300 nm for pure Ni (Neishi et al., 2002)), in that the former can sustain a higher σ_e. Given that d_s is achieved under the balance between hardening and recovery as mentioned before, it is reasonable to surmise that the stress ratio $\eta_{Stress} = 1$ can be taken as a signature for d_s from the phenomenological perspective. Interestingly, it seems in Fig. 8(a) that at a given σ_e, a greater f leads to a smaller d_s. In other words, to refine or coalesce the grains to a fixed size d_s, the NT metals with a higher f

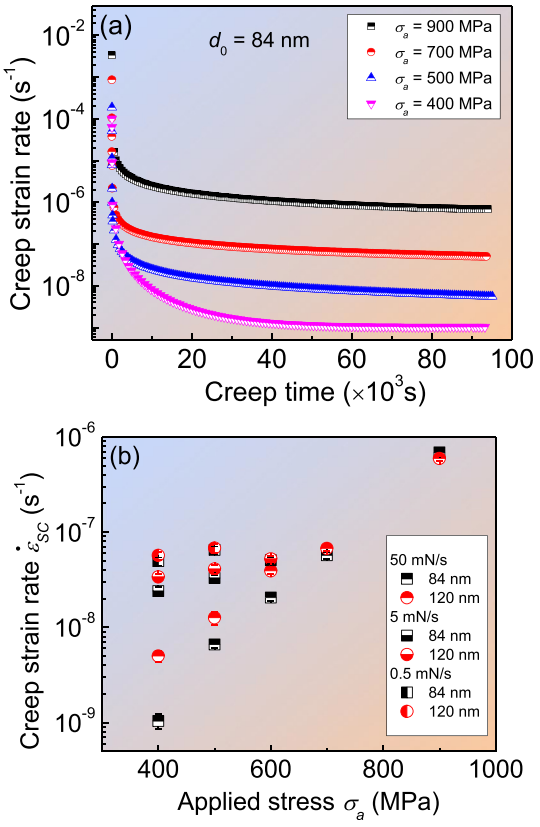

Fig. 6. (a) Creep strain rate of d_0 ~84 nm NT Ni as a function of holding time loaded at a loading rate of 50 mN·s^{-1} and held at different σ_a; (b) Variations in steady-state creep stain rate $\dot{\varepsilon}_{SC}$ with increasing σ_a at different loading rates.

need a much lower σ_e compared with their nontwinned counterparts. These results imply that the fraction of nanotwins f plays a significant role in either refinement or growth of grains, as supported by most of the findings that twins can facilitate grain refinement/growth (Luo et al., 2014; Cao et al., 2015). In contrast, in Fig. 8(b), one can clearly see that at a given σ_e, a smaller λ results in a smaller d_s; namely, the NT samples with smaller λ are much easier to reach a d_s under a lower σ_e, which suggests that the twin thickness λ also plays an important role in both the refinement of grains with $d > d_s$ and the coalescence of grains with $d < d_s$. The present findings imply that tuning f and λ can effectively manipulate the d_s, thereby benefiting to significantly enhance the mechanical strength of NT metals (*e.g.*, Ni, Cu). If d_0 in either twinned or nontwinned metals is larger than the predicted d_s, they will refine; otherwise, they will coarsen.

The current strain rate-independent grain growth to a saturated or stable size d_s ~220 ± 20 nm at low stress levels in the present NT Ni with high SFE and the reported grain coarsening in NT Cu (Brons et al., 2013) with medium SFE deformed at

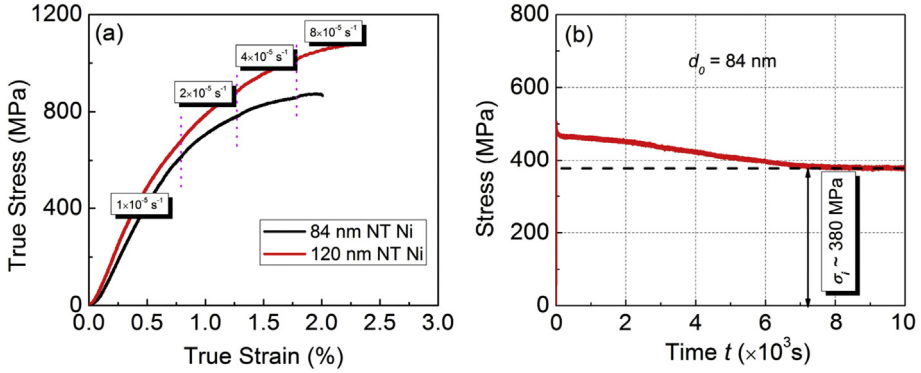

Fig. 7. Results of the internal stress σ_i measured by two different experimental methods: (a) strain rate jump experiment and (b) full stress relaxation test. The σ_i values obtained for NT Ni at room temperature in jump tests are ~380 MPa for d_0~84 nm and ~385 MPa for d_0 ~120 nm, respectively, the same as those obtained from stress relaxation experiments.

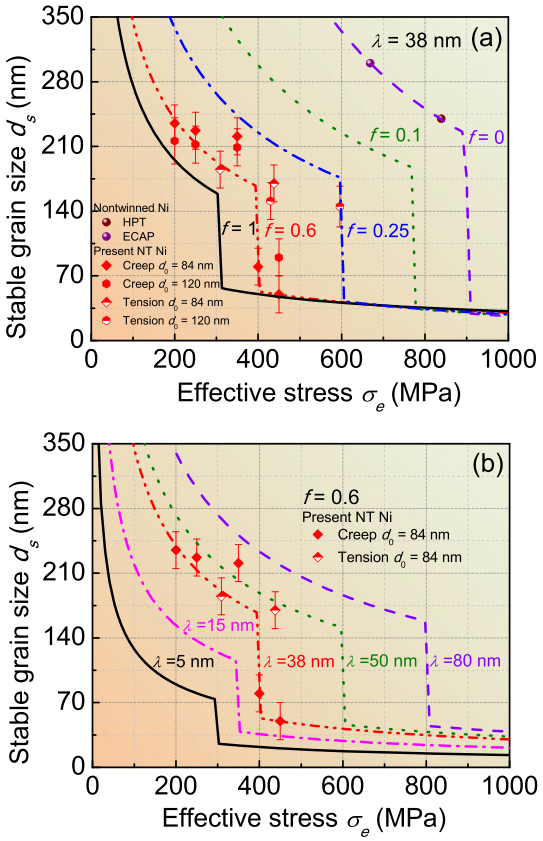

Fig. 8. Calculated stable grain size d_s as a function of effective stress σ_e in nanograined Ni with different f (a) and λ (b). In (a), the present experimental data are compared with the reported d_s of nontwinned Ni obtained from HPT (Edalati and Horita, 2011), and ECAP (Neishi et al., 2002), and with those of NT Ni obtained from our uniaxial tensile test (Li et al., 2015). In (b), d_s of 84 nm NT Ni samples after creep at different σ_a are compared with those after tensile tests (Li et al., 2015).

cryogenic temperature indicate the athermal nature of grain growth in nanostructured NT metals, and suggest that the applied stress σ_a is larger than the internal stress σ_i to activate dislocation motion. Namely, it appears that grain growth is controlled by the ratio of non-zero stress σ_e to σ_i in metals. Indeed, for our creep tests associated with constant σ_a, grain growth is achieved under the condition that the non-zero σ_e is far less than σ_i, *i.e.*, stress ratio $\eta_{Stress} = \sigma_e/\sigma_i < 1$. This is reasonable, because the nanosized grains with $d < d_s$ provide insufficient room for dislocation pile-ups to form dislocation substructures (*e.g.*, dislocation tangles, cells and walls) which are needed for grain refinement (Wang et al., 1995), in particular under a lower σ_e. To fulfill grain refinement, the stress ratio $\eta_{Stress} = \sigma_e/\sigma_i > 1$ is required to enable the emergence of dislocation substructures (or subgrain boundaries) through dislocation pile-ups and their interactions, as supported by solid experimental findings of grain refinement based on severe plastic deformation (Edalati and Horita, 2011; Mohamed, 2003), such as ball milling, HPT and ECAP. Similarly, our present NT Ni foils also exhibit grain refinement under the high stress level since the non-zero σ_e is larger than σ_i, *i.e.*, stress ratio $\eta_{Stress} = \sigma_e/\sigma_i > 1$. A most recent study on bulk NC Cu tested by systematic loading-unloading compressive cyclic experiments has reported a similar phenomenon by Hu et al. (2016), in which grain growth occurs under the condition of $\eta_{Stress} \approx 0.5$, whereas grain refinement occurs at $\eta_{Stress} \approx 2.5$. Therefore, we tentatively propose a new parameter, *i.e.*, $\eta_{Stress} = \sigma_e/\sigma_i$, to characterize the grain size evolution behavior, which also reflects the competition between effective and internal stresses, as schematically displayed in Fig. 9. This figure schematically illustrates that grains in nanostructured metals undergoing creep or fatigue deformation associated with $\eta_{Stress} < 1$ are preferred to grow to d_s, whereas the CG metals undergoing severe plastic deformation associated with $\eta_{Stress} > 1$ are favorable to shrink their grains (or form dislocation substructures, *e.g.*, dislocation cells/walls) to d_s, and the stable size d_s is reached at the stress ratio of $\eta_{Stress} = 1$, as verified in the present experimental TEM observations and further discussed in terms of the steady-state creep strain rate below.

5.2. Quantifying the steady-state creep strain rate

At present, it has been well established that a unified theory of steady-state creep incorporates two competing effects, *i.e.*, work hardening and recovery softening (Kassner, 2009). Based on this theory, Eq. (15) reveals that $\dot{\varepsilon}_{SC}$ is closely related to σ_e and material parameters such as μ, Ω, D, γ, θ, d and λ in Section 2, which captures well the scaling behavior of $\dot{\varepsilon}_{SC}$ with σ_e by

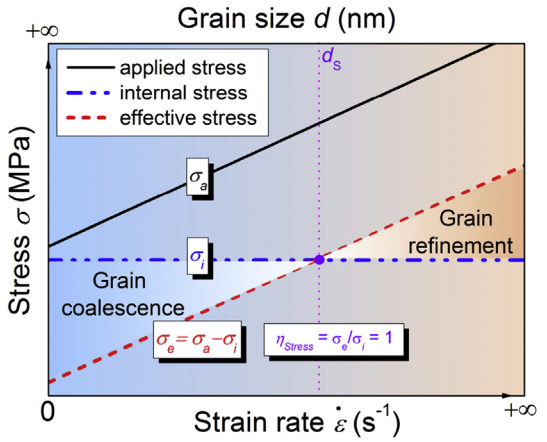

Fig. 9. Schematic illustration of grain growth based on the competition between σ_i and the σ_e. The ratio of σ_e to σ_i, η_{Stress}, is used to evaluate the grain size evolution: $\eta_{Stress} < 1$, grains coarsen; $\eta_{Stress} > 1$, grains refine; and at $\eta_{Stress} = 1$, a stable grain size is reached.

considering the following values of parameters: $\upsilon = 0.31$, $\mu = 94.7$ GPa, $\gamma = 125$ mJ m^{-2}, $b = 0.249$ nm, $\Omega = 1.1 \times 10^{-29}$ m^{-3}, $D = 3.26 \times 10^{-25}$ m^3 s^{-1} (Choi et al., 2013), $k = 1.38 \times 10^{-23}$ J K^{-1}, $T = 298$ K, $\theta = 10°$ (for low-angle GBs), $\beta = 0.08$ and 0.09 for d_0 ~84 nm and 120 nm NT Ni, respectively (see Fig. 10(a)). The consistency between dislocation model and experimental findings for both d_s and $\dot{\varepsilon}_{SC}$ in the present NT Ni suggests the great predictive capacity of this model by considering dislocation emission from boundaries in nanostructures. Owing to the differences in the microstructural evolution such as d, λ and f between d_0 ~84 nm and 120 nm NT Ni, there exists a crossover of $\dot{\varepsilon}_{SC}$ with increasing σ_a or σ_e, and $\dot{\varepsilon}_{SC}$ in larger grain sized NT Ni is relatively higher under the low stress level, contrary to that under high stress level (see Fig. 10(a)). In fact, these different internal features can significantly alter the mechanical response of NT metals, contrary to the general opinion reported earlier (Lu et al., 2009a; Li et al., 2010; Li et al., 2015).

In addition, it is very important to quantitatively estimate the internal stress during creep, in particular at the steady-state creep stage, and to illustrate the relationship between σ_i and σ_e or the variation of the stress ratio η_{Stress}. The initial dislocation densities under different σ_a spanning from 400 MPa to 900 MPa, to a first approximation, can be roughly considered as the same. Taking a series of the same parameters as above: $M_T = 3.06$, $\upsilon = 0.31$, $\mu = 94.7$ GPa, $b = 0.249$ nm, and $\theta = 10°$, the variation in stress σ_i as well as σ_e with time t calculated with Eq. (18) under different σ_a are displayed in Fig. 10(b) for d_0 ~84 nm NT Ni as an example. It is found that the calculated σ_i, opposite to σ_e, first decreases (low stress level ~400 MPa) or increases (high stress level ~900 MPa) with increasing time and then almost reaches a stress plateau in the whole time scale. These two curves intercross at a critical time, beyond which the creep transits from the primary creep stage to the steady-state creep stage and is comparable with the experimental findings in the studied stress levels spanning from 400 to 900 MPa. At this calculated critical time, the stress ratio $\eta_{Stress} = 1$, the steady-state creep stage as well as the stable microstructure characteristics (*e.g.*, d_s) begin to be observed. The coincidence of the stress ratio $\eta_{Stress} = 1$ obtained from both the experimental observation of d_s and the theoretical calculation of σ_i, albeit the significance of which should not be overestimated, implies a potential intrinsic correlation between $\eta_{Stress} = 1$ and the dynamic balanced characteristics such as d_s and $\dot{\varepsilon}_{SC}$ in metals during plastic deformation.

5.3. Grain growth and grain refinement via dislocation–boundary interactions

It is generally understood that the twin thickness λ increases with the increase of the grain size d. However, our experimental results show the opposed manifestation, as seen from Fig. 3. This can be explained in terms of the energy difference between formation energy of the incoherent TB (ITB) (W_{ITB}) and that of CTB (W_{CTB}), as proposed by Xue et al. (2015). When $W_{ITB} > W_{CTB}$, it is energetically feasible to extend the inclined growth twins; In contrast, when $W_{ITB} < W_{CTB}$, the continuous growth of CTBs becomes energetically unfavorable, and the nanotwins or the NT system is unstable (Xue et al., 2015). In our NT Ni foils prepared by a pulse electrodeposition technique under nonequilibrium conditions, most of the twins are terminated at GBs and likely store excessive energy in these abundant CTBs. In this regard, during subsequent deformation, the unstable/metastable nanotwinned structures likely exhibit detwinning behavior in the form of reduced λ along with grain growth to reach the stable microstructures. This is a possible reason why we observed the larger sized grains contain smaller sized twins in the NT Ni samples in the current work, opposite to the general belief.

In general, a metal with higher SFE is more difficult to twin or detwin during plastic deformation (Zhu et al., 2011). However, a remarkable increase in f and a notable variation in λ are observed in the present NT Ni tested under low stresses, as signatures of the (de)twinning process. Therefore, it is normally anticipated that both grain growth and grain refinement in NT metals can be achieved via twinning and its reverse process, *i.e.*, detwinning. With regard to the underlying mechanism(s)

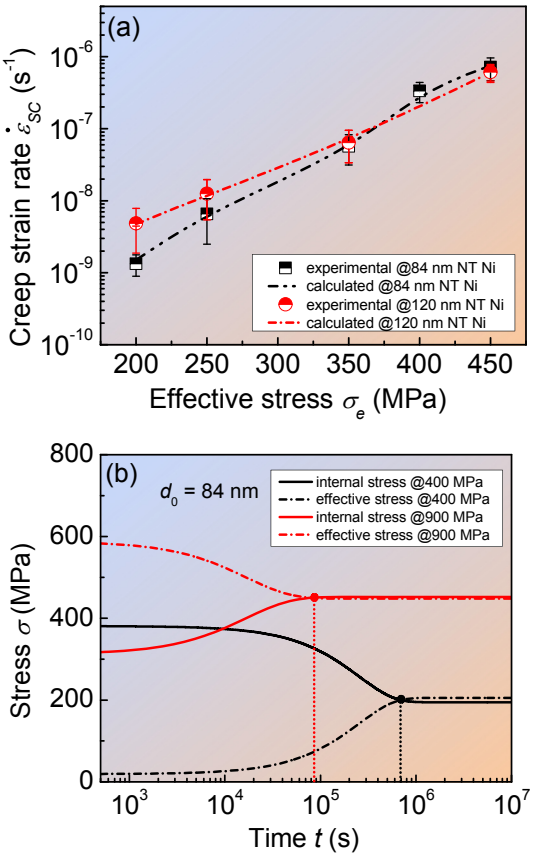

Fig. 10. (a) Experimental $\dot{\varepsilon}_{SC}$ (half circle and half square symbols) as a function of σ_e, which can be captured well by the present model (black and red lines); (b) Theoretically predicted trend of the variation in σ_i and σ_e with time during creep under 400 MPa and 900 MPa of d_0~84 nm NT Ni. (For interpretation of the references to colour in this figure legend, the reader is referred to the web version of this article.)

of grain growth and grain refinement in our NT Ni foils during plastic deformation, we proposed that it is achieved by (de) twinning via dislocation–boundary interactions, similar to the case of dislocation-TB interactions (Jin et al., 2008; Zhu et al., 2011; Wang et al., 2010, 2012).

Fig. 11 schematically illustrates the interaction of dislocations with GBs/TBs leading to grain growth and grain refinement. An incoming extended dislocation emitted from GB source *A* in grain 1 (G1) can completely transfer across the (Σ3) GB and then dissociate into three Shockley partials, among of which two partials glide on the slip plane in another grain (G2), bounding a stacking fault, and the third "GB dislocation$\frac{a}{6}<121>_{GB}$" is left within the (Σ3) GB, following $\frac{a}{2}[101]_{G1}\rightarrow\frac{a}{2}[101]_{G2}+\frac{a}{6}[121]_{GB}\rightarrow\frac{a}{6}[211]_{G2}+\frac{a}{6}[1\bar{1}2]_{G2}+\mathrm{SF}+\frac{a}{6}[121]_{GB}$ (Jin et al., 2008). This can reduce the misorientation angle between adjacent grains and facilitate GB motion, thus promoting grain growth (Bachurin et al., 2010; Li et al., 2015). Alternatively, the extended dislocation emitted from GB source *B* in G1 can interact with the (Σ3) GB and dissociate into a new partial in G2 and a Frank dislocation at GB, following the dislocation reaction $\frac{a}{2}[101]_{G1}\rightarrow\frac{a}{6}[1\bar{2}1]_{G2}+\frac{a}{3}[111]_{GB}$. The Frank dislocation at GB can transmit across GB, releasing a partial dislocation in G2 and a perfect dislocation accompanied with a residual dislocation at GB, yielding $\frac{a}{3}[111]_{GB}\rightarrow\frac{a}{6}[\bar{1}2\bar{1}]_{G2}+\frac{a}{2}[101]_{GB}+\delta_{GB}$. Similarly, the GB residual dislocation can also reduce the misorientation angle between grains and facilitate GB motion, thereby rendering grain growth (Bachurin et al., 2010; Li et al., 2015). In the above mentioned two mechanisms of twinning-assisted grain growth, the former does not involve the formation of a twin in the nearby grain, as well as the residual Frank sessile dislocation at GB, while in the latter, the twin can penetrate into another grain via the repeated slip of partials.

In the case of detwinning-induced grain refinement, a full dislocation emitted from GB source *C* can dissociate into partials associated with a SF, or a partial dislocation directly emit from the source *C*. These partials would interact with the primary TB to generate (de)twinning partials with Burgers vectors parallel to primary TB during the interactions of secondary twins/SFs with primary TB (*e.g.*, $\frac{a}{6}[1\bar{1}2]_M\rightarrow\frac{a}{6}[011]_{TB}+\frac{a}{6}[1\bar{2}1]_{TB}$, where subscripts "*M*" stands for matrix) (Zhu et al., 2011; Cao et al., 2015), resulting in detwinning of the primary twins via gliding of detwinning partials $\frac{a}{6}<1\bar{2}1>_{TB}$ and producing very high densities of sessile dislocations $\frac{a}{6}<110>_{TB}$. The accumulation of these remnant dislocations will produce a new GB with neighboring

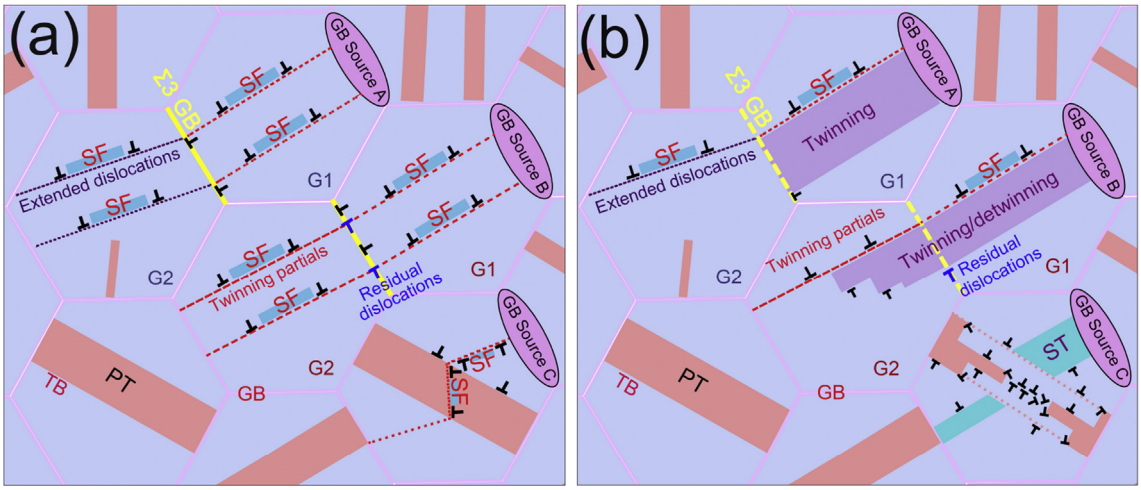

Fig. 11. Schematic illustration of twinning/detwinning-associated grain growth and grain refinement (b) via dislocation-GBs/TBs interactions (a). For the twinning/detwinning-mediated grain growth, the incoming extended dislocations or the partials, emitted from GB Source *A* or *B*, can trigger the twinning/detwinning processes via dislocation-GB reactions, thereby leading to grain growth. In the case of detwinning-mediated grain refinement, the partials, emitted from GB Source *C* or produced by the dissociation of a perfect dislocation, will result in the detwinning of the primary twin via dislocation-TB reactions associated with the formation of a low-angle GB by the remnant dislocations from the detwinning of primary twins. See text for detailed interpretations. (SF: stacking fault; PT: primary twin; ST: secondary twin; GB: grain boundary; TB: twin boundary.)

grains having similar orientations, as uncovered in low SFE metals such as the austenitic duplex stainless steel (Cao et al., 2015).

Specifically, it is worth noting that under low stresses twinning mediated grain growth accompanied with significantly enhanced f emerges in NT Ni with high SFE, whereas detwinning dominated grain refinement accompanied with remarkably reduced λ occurs under high stresses. Actually, these interesting phenomena can be explained in the light of plastic relaxation of the internal stress in a twin (Barnett et al., 2013b), which is characterized by a plastic relaxation factor ξ, *i.e.*, $\xi = 1 - \frac{\tau_i - \tau_e}{2\mu s q}\left(1 + \frac{11q}{5}\right)$, where s is the magnitude of the twinning shear and q is the twin thickness-to-length ratio (or aspect ratio, and $q = \left|(5\tau_e)/\left[10\mu s\zeta(1 - {\eta_{Stress}}^2) - 11\tau_e\right]\right|$, ζ is a factor of ~0.1–0.6). It appears that if σ_e is closer to σ_i, the relaxation of the twin back stress is greater via the dislocation-nucleation dominated microyielding. In such a case, when twin systems are favorably aligned in adjacent grains, nanotwins can rapidly propagate over the structure as the secondary twinning event relaxes the back stress in the primary (triggering) twin to achieve grain growth. Indeed, the NT Ni foils tested under higher stress (~900 MPa) reach the steady state much faster as observed in Fig. 6(a), implying greater stress relaxation. The almost identical f (~85%) in the NT Ni samples tested in the stress range of 400–700 MPa likely suggests that relaxation of the twin back stress is independent on the applied stress in high SFE metals. In contrast, if σ_e exceeds σ_i, full plasticity surrounding the matrix owing to dislocation glide would lead to complete relaxation of the twin back stress (Barnett et al., 2013b), rendering the dislocation-transmission dominated macroyielding to achieve detwinning-induced grain refinement. Specifically, as the critical stress for twinning dislocation motion is satisfied in the reverse direction, twin shrinkage would emerge (Barnett et al., 2013a).

6. Summary

The present findings hopefully convey the valuable information that the microstructural evolution in NT Ni with high SFE after creep is highly correlated with twinning/detwinning via dislocation-GB/TB interactions, which plays a key role in changing local grain orientation and dissociating boundaries of nanograins to facilitate grain growth/refinement and plastic deformation. The proposed parameter of effective-to-internal stress ratio η_{Stress} can characterize the microstructural evolution, that is to say, if $\eta_{Stress} < 1$, grains coarsen; $\eta_{Stress} > 1$, grains refine; and at $\eta_{Stress} = 1$, a stable grain size is reached. The dislocation-based model quantifying the stable grain size and the steady-state creep strain rate provides mechanistic insight into the fundamental understanding of mechanical stress-driven grain growth and refinement in metals to achieve performance optimization via tuning their microstructural features.

Acknowledgments

This work was supported by the 111 Project of China (B06025) and the National Natural Science Foundation of China (Grant Nos. 51201123, 51322104, 51321003 and 51571157). GL thanks the support from the National Science Find for Distinguished

Yong Scholars. JYZ is grateful for Natural Science Basic Research Plan in Shaanxi Province of China (Program No. 2015JM5158) and China Postdoctoral Science Foundation (2016M590940) for part of financial support.

References

Ahlquist, C.N., Gascaneri, R., Nix, W.D., 1970. A phenomenological theory of steady state creep based on average internal and effective stresses. Acta Metall. 18, 663–671.
Anderoglu, O., Misra, A., Wang, J., Hoagland, R., Hirth, J.P., Zhang, X., 2010. Plastic flow stability of nanotwinned Cu foils. Int. J. Plast. 26, 875–886.
Argon, A.S., Takeuchi, S., 1981. Internal stresses in power-law creep. Acta Metall. 29, 1877–1884.
Bachurin, D.V., Weygand, D., Gumbsch, P., 2010. Dislocation-grain boundary interaction in <111> textured thin metal films. Acta Mater. 58, 5232–5241.
Barai, P., Weng, G.J., 2008. Mechanics of creep resistance in nanocrystalline solids. Acta Mech. 195, 327–348.
Barnett, M., Setty, M., Siska, F., 2013a. Estimating critical stresses required for twin growth in a magnesium Alloy. Metall. Mater. Trans. A 44, 2962–2969.
Barnett, M., Stanford, N., Ghaderi, A., Siska, F., 2013b. Plastic relaxation of the internal stress induced by twinning. Acta Mater. 61, 7859–7867.
Basirat, M., Shrestha, T., Potirniche, G.P., Charit, I., Rink, K., 2012. A study of the creep behavior of modified 9Cr1Mo steel using continuum-damage modeling. Int. J. Plast. 37, 95–107.
Blum, W., Li, Y., 2007. Flow stress and creep rate of nanocrystalline Ni. Scr. Mater. 57, 429–431.
Brons, J.G., Padilla, H., Thompson, G.B., Boyce, B., 2013. Cryogenic indentation-induced grain growth in nanotwinned copper. Scr. Mater. 68, 781–784.
Caillard, D., Martin, J., 2003. Thermally Activated mechanisms in crystal plasticity. Pergamon Mater. Ser. Elsevier Sci. 8.
Cao, Y., Wang, Y., An, X., Liao, X., Kawasaki, M., Ringer, S., Langdon, T.G., Zhu, Y., 2015. Grain boundary formation by remnant dislocations from the de-twinning of thin nano-twins. Scr. Mater. 100, 98–101.
Carlton, C.E., Ferreira, P.J., 2007. What is behind the inverse Hall–Petch effect in nanocrystalline materials? Acta Mater. 55, 3749–3756.
Chauhan, M., Mohamed, F.A., 2007. Microstructural evolution of bulk nanocrystalline Ni during creep. J. Mater. Sci. 42, 1606–1614.
Cheng, S., Zhao, Y., Wang, Y.M., Li, Y., Wang, X., Liaw, P., Lavernia, E., 2010. Structure modulation driven by cyclic deformation in nanocrystalline NiFe. Phys. Rev. Lett. 104, 255501.
Choi, C.H., Kim, Y.J., Seok, M., Yoo, B., Kim, J., Wang, Y.M., Jang, J., 2013. Nanoscale room temperature creep of nanocrystalline nickel pillars at low stresses. Int. J. Plast. 41, 53–64.
Conrad, H., 1970. The athermal component of the flow stress in crystalline solids. Mater. Sci. Eng. 6, 265–273.
Eckert, J., Holzer, J., Krill, C., Johnson, W., 1992. Structural and thermodynamic properties of nanocrystalline fcc metals prepared by mechanical attrition. J. Mater. Res. 7, 1751–1761.
Edalati, K., Horita, Z., 2011. High-pressure torsion of pure metals: influence of atomic bond parameters and stacking fault energy on grain size and correlation with hardness. Acta Mater. 59, 6831–6836.
Ekh, M., Bargmann, S., Grymer, M., 2011. Influence of grain boundary conditions on modeling of size-dependence in polycrystals. Acta Mech. 218, 103–113.
Friedel, J., 1964. Dislocations. Pergamon Press, Oxford.
Gianola, D.S., Van Petegem, S., Legros, M., Brandstetter, S., Van Swygenhoven, H., Hemker, K.J., 2006. Stress-assisted discontinuous grain growth and its effect on the deformation behavior of nanocrystalline aluminum thin films. Acta Mater. 54, 2253–2263.
Gollapudi, S., Rajulapati, K., Charit, I., Koch, C., Scattergood, R., Murty, K., 2010. Creep in nanocrystalline materials: role of stress assisted grain growth. Mater. Sci. Eng. A 527, 5773–5781.
Guiu, F., Pratt, P., 1964. Stress relaxation and the plastic deformation of solids. Phys. Stat. Sol. 6, 111–120.
Guo, N., Zhang, J.Y., Cheng, P., Liu, G., Sun, J., 2013. Room temperature creep behavior of free-standing Cu films with bimodal grain size distribution. Scr. Mater. 68, 849–852.
Gurtin, M., 2008. A theory of grain boundaries that accounts automatically for grain misorientation and grain-boundary orientation. J. Mech. Phys. Sol. 56, 640–662.
Hasegawa, T., Ikeuchi, Y., Karashima, S., 1972. Internal stress and dislocation structure during sigmoidal transient creep of a Copper-16 at. % Aluminium alloy. Metal. Sci. J. 6, 78–82.
Hirth, J.P., Lothe, J., 1982. Theory of Dislocations, second ed. Krieger Publishing Company Malabar, Florida.
Hu, J., Zhang, J., Jiang, Z., Ding, X., Zhang, Y., Han, S., Sun, J., Lian, J., 2016. Plastic deformation behavior during unloading in compressive cyclic test of nanocrystalline copper. Mater. Sci. Eng. A 651, 999–1009.
Jin, Z.H., Gumbsch, P., Albe, K., Ma, E., Lu, K., Gleiter, H., Hahn, H., 2008. Interactions between non-screw lattice dislocations and coherent twin boundaries in face-centered cubic metals. Acta Mater. 56, 1126–1135.
Kassner, M.E., 2009. Fundamentals of Creep in Metals and Alloys. Elsevier, Oxford.
Kassner, M.E., Geantil, P., Levine, L., 2013. Long range internal stresses in single-phase crystalline materials. Int. J. Plast. 45, 44–60.
Kim, J.-Y., Jang, D., Greer, J.R., 2011. Nanolaminates utilizing size-dependent homogeneous plasticity of metallic glasses. Adv. Funct. Mater. 21, 4550–4554.
Kocks, U.F., Argon, A.S., Ashby, M., 1975. Thermodynamics and kinetics of slip. Prog. Mater. Sci. 19, 1–281.
Kruml, T., Coddet, O., Martin, J., 2008. About the determination of the thermal and athermal stress components from stress-relaxation experiments. Acta Mater. 56, 333–340.
Kumar, K.S., Suresh, S., Chisholm, M., Horton, J., Wang, P., 2003. Deformation of electrodeposited nanocrystalline nickel. Acta Mater. 51, 387–405.
Li, J., Zhang, J.Y., Jiang, L., Zhang, P., Wu, K., Liu, G., Sun, J., 2015. Twinning/detwinning-mediated grain growth and mechanical properties of free-standing nanotwinned Ni foils: grain size and strain rate effects. Mater. Sci. Eng. A 628, 62–74.
Li, J.C.M., 1967. Dislocation dynamics in deformation and recovery. Can. J. Phys. 45, 493–509.
Li, J.C.M., Chou, Y.T., 1970. The role of dislocations in the flow stress grain size relationships. Metall. Mater. Trans. 1, 1145–1159.
Li, X., Wei, Y., Lu, L., Lu, K., Gao, H., 2010. Dislocation nucleation governed softening and maximum strength in nano-twinned metals. Nature 464, 877–880.
Li, Y., Zhang, Y., Tao, N., Lu, K., 2009. Effect of the Zener-Hollomon parameter on the microstructures and mechanical properties of Cu subjected to plastic deformation. Acta Mater. 57, 761–772.
Lu, L., Chen, X., Huang, X., Lu, K., 2009a. Revealing the maximum strength in nanotwinned copper. Science 323, 607–610.
Lu, L., Zhu, T., Shen, Y.F., Dao, M., Lu, K., Suresh, S., 2009b. Stress relaxation and the structure size-dependence of plastic deformation in nanotwinned copper. Acta Mater 57, 5165–5173.
Lu, N., Du, K., Lu, L., Ye, H.Q., 2015. Transition of dislocation nucleation induced by local stress concentration in nanotwinned copper. Nat. Commun. 6, 7648.
Luo, X., Zhu, X., Zhang, G., 2014. Nanotwin-assisted grain growth in nanocrystalline gold films under cyclic loading. Nat. Commun. 5, 3021.
Mohamed, F.A., 2003. A dislocation model for the minimum grain size obtainable by milling. Acta Mater. 51, 4107–4119.
Mompiou, F., Caillard, D., Legros, M., Mughrabi, H., 2012. In situ TEM observations of reverse dislocation motion upon unloading in tensile-deformed UFG aluminium. Acta Mater. 60, 3402–3414.
Neishi, K., Horita, Z., Langdon, T.G., 2002. Grain refinement of pure nickel using equal-channel angular pressing. Mater. Sci. Eng. A 325, 54–58.
Orlová, A., Čadek, J., 1986. Dislocation structure in the high temperature creep of metals and solid solution alloys: a review. Mater. Sci. Eng. 77, 1–18.
Orlová, A., Pahutová, M., čadek, J., 1972. Dislocation structure and applied, effective and internal stress in high-temperature creep of alpha iron. Philos. Mag. 25, 865–877.
Rupert, T.J., Gianola, D.S., Gan, Y., Hemker, K.J., 2009. Experimental observations of stress-driven grain boundary migration. Science 326, 1686–1690.
Upmanyu, M., Srolovitz, D., Shvindlerman, L., Gottstein, G., 2002. Molecular dynamics simulation of triple junction migration. Acta Mater. 50, 1405–1420.
Van Swygenhoven, H., Derlet, P., Hasnaoui, A., 2002. Atomic mechanism for dislocation emission from nanosized grain boundaries. Phys. Rev. B 66, 024101.

Van Swygenhoven, H., Derlet, P., Frøseth, A., 2006. Nucleation and propagation of dislocations in nanocrystalline fcc metals. Acta Mater 54, 1975–1983.
Van Swygenhoven, H., Farkas, D., Caro, A., 2000. Grain-boundary structures in polycrystalline metals at the nanoscale. Phys. Rev. B 62, 831–838.
Wang, B., Idrissi, H., Galceran, M., Colla, M., Turner, S., Hui, S., Raskin, J., Pardoen, T., Godet, S., Schryvers, D., 2012. Advanced TEM investigation of the plasticity mechanisms in nanocrystalline freestanding palladium films with nanoscale twins. Int. J. Plast. 37, 140–156.
Wang, J., Li, N., Anderoglu, O., Zhang, X., Misra, A., Huang, J., Hirth, J.P., 2010. Detwinning mechanisms for growth twins in face-centered cubic metals. Acta Mater. 58, 2262–2270.
Wang, N., Wang, Z.R., Aust, K.T., Erb, U., 1995. Effect of grain size on mechanical properties of nanocrystalline materials. Acta Metall. Mater. 3, 519–528.
Wang, Y.M., Hamza, A., Ma, E., 2006. Temperature-dependent strain rate sensitivity and activation volume of nanocrystalline Ni. Acta Mater. 54, 2715–2726.
Wang, Y.M., Sansoz, F., LaGrange, T., Ott, R., Marian, J., Barbee Jr., T., Hamza, A., 2013. Defective twin boundaries in nanotwinned metals. Nat. Mater. 12, 697–702.
Winning, M., Gottstein, G., Shvindlerman, L., 2002. On the mechanisms of grain boundary migration. Acta Mater. 50, 353–363.
Xue, S., Fan, Z., Chen, Y., Li, J., Wang, H., Zhang, X., 2015. The formation mechanisms of growth twins in polycrystalline Al with high stacking fault energy. Acta Mater. 101, 62–70.
Zhao, Y., Fang, Q., Liu, Y., Wen, P., Liu, Y., 2015. Creep behavior as dislocation climb over NiAl nanoprecipitates in ferritic alloy: the effects of interface stresses and temperature. Int. J. Plast. 69, 89–101.
Zhu, B., Asaro, R.J., Krysl, P., Bailey, R., 2005. Transition of deformation mechanisms and its connection to grain size distribution in nanocrystalline metals. Acta Mater. 53, 4825–4838.
Zhu, Y., Li, Z., Huang, M., Liu, Y., 2015. Strengthening mechanisms of the nanolayered polycrystalline metallic multilayers assisted by twins. Int. J. Plast. 72, 168–184.
Zhu, Y., Wu, X., Liao, X., Narayan, J., Kecskés, L., Mathaudhu, S., 2011. Dislocation-twin interactions in nanocrystalline fcc metals. Acta Mater. 59, 812–821.